Uncertainty Quantification for Applications of ^{239}Pu Fission Cross Sections Using a Monte Carlo Technique

T. Kawano, K.M. Hanson, S.C. Frankle, P. Talou, M.B. Chadwick, R.C. Little

Los Alamos National Laboratory

We present an approach to uncertainty quantification for nuclear applications, which combines the covariance evaluation of differential cross-sections data and the error propagation from matching a criticality experiment using a neutron-transport calculation. We have studied the reduction in uncertainty of ^{239}Pu fission cross sections by using a one-dimensional neutron-transport calculation with the PARTISN code. The evaluation of ^{239}Pu differential cross-section data is combined with a criticality measurement (Jezebel) using a Bayesian method. To quantify the uncertainty in such calculations, we generate a set of random samples of the cross sections, which represents the covariance matrix, and estimate the distribution of calculated quantities, such as criticality. We show that inclusion of the Jezebel data reduces uncertainties in estimating neutron multiplicity.

We present an approach to uncertainty quantification for nuclear applications, which combines the covariance evaluation of differential cross-sections data and the error propagation from matching a criticality experiment using a neutron-transport calculation. We have studied the reduction in uncertainty of ^{239}Pu fission cross sections by using a one-dimensional neutron-transport calculation with the PARTISN code. The evaluation of ^{239}Pu differential cross-section data is combined with a criticality measurement (Jezebel) using a Bayesian method. To quantify the uncertainty in such calculations, we generate a set of random samples of the cross sections, which represents the covariance matrix, and estimate the distribution of calculated quantities, such as criticality. We show that inclusion of the Jezebel data reduces uncertainties in estimating neutron multiplicity.

I INTRODUCTION

Advanced technologies of nuclear energy applications require uncertainty quantification (UQ) to assess the margin in a design and to validate model predictions, such as a neutron-transport calculation for criticality. The neutron-transport calculation may have two main sources of uncertainty, the nuclear data used and the modeling itself. When a covariance of nuclear data is provided, the uncertainty in a calculated quantity (e.g., neutron multiplicity, $k_{\rm eff}$, for example) can be estimated by propagating the error in the nuclear data to the outputs of the application code. The model uncertainty is not discussed in this paper since this is outside our scope.

Ishikawa et al.[1] adjusted group cross sections and other nuclear data such as ν_p to match integral data obtained from many critical systems. The adjusted cross-section library with their covariance makes it possible to predict the uncertainty in the transport calculations if the computation of the sensitivity is feasible. In general, however, calculation of the error propagation is difficult to perform, since many application codes, such as a neutron-transport Monte Carlo simulation codes, require tremendous computing capabilities.

To perform the uncertainty quantification for such calculations within a realistic computational resource (time), a feasible method must be developed. One possible solution is to perform the calculations with several perturbed cross-section sets (ensemble), then look at the distribution of the calculated quantities. In this Monte Carlo technique, we must be careful about the fact that the uncertainties in the cross sections are not independent, and this information must be included into the sample set as a constraint.

The constraint is a result of nuclear data evaluation, and it is expressed as a data covariance. For example, when cross sections are evaluated based on experimental data having an unknown normalization, the evaluated data-correlation must be positive, because the unknown normalization error propagates to all the evaluated energy points in a similar way. With this covariance, if the fluctuations in the cross section tend to be larger than the averaged (unperturbed) value at a certain energy, cross sections at the other energies also tend to be larger. Therefore, a key issue of our Monte Carlo procedure is to properly evaluate the covariance of nuclear data.

In this study we evaluated the covariance of ^{239}Pu fission cross section, because a large experimental database to evaluate the covariance is available, and a straightforward application of ^{239}Pu fission cross section such as Jezebel — a critical assembly at LANL[2, 3] — makes it possible to validate our Monte Carlo method. In Sec. 2, the covariance for ^{239}Pu fission cross section is evaluated from differential measurements of the $^{239}\mathrm{Pu}(n, f)$ reaction. It is known that the Los Alamos evaluated ^{239}Pu fission cross-section data reproduce most integral measurements very well. With a Bayesian technique[4], such integral data can be included in the covariance data to constrain the differential cross sections, which is described in Sec. 3. In Sec. 4, we generate an ensemble of cross sections according to the covariances, and perform a one-dimensional neutron transport calculations with this ensemble to investigate the distribution of the neutron multiplicity k_{eff}, which is an estimate of the uncertainty in the nuclear data application. The neutron transport calculations are performed with the PARTISN code[5]. Although we limit ourselves to a computationally fast transport calculation to demonstrate our procedure, the Monte Carlo method can be used in any type of application codes.

II ESTIMATION OF UNCERTAINTIES BY USING DIFFERENTIAL EXPERIMENTAL DATA

Uncertainties in evaluated cross sections originate from the experimental data used. The ^{239}Pu fission cross sections evaluated at LANL[6] are also based on measurements of differential data, and the uncertainties (covariance) of the cross sections can be deduced from the experimental uncertainties. However, many of the ^{239}Pu fission cross sections were measured as a ratio to ^{235}U fission cross section, which is so-called a standard cross section[7], and a choice of this standard cross section affects the evaluation of ^{239}Pu fission cross section and its covariance.

The standard evaluation for ENDF/B-VII has been completed recently at IAEA[7], but the final covariance data have not yet been released. Here we adopt an interim standard data[8] for ^{235}U fission cross section for which we do not expect a large difference from the final values. With this standard, all the ratio measurements are converted into absolute ^{239}Pu fission cross section values.

In the IAEA standard evaluation, all existing experimental data used in the evaluation were also examined carefully, and covariance for the measurements in each experiment was assigned. We adopt this experimental database, together with the IAEA interim standard cross section, to generate a covariance matrix for ^{239}Pu fission cross section.

In this procedure, the experimental database is not the same as what we used for ^{239}Pu fission cross section evaluation at LANL[6]. However, the limitation arising from this approximation might be mitigated, because we do not use a point-wise cross section but a group-averaged cross section in this study. Information from individual experiments is diluted inasmuch as each group often contains a large number of experimental data points. The 30-group structure adopted in the LANL MENDF6 multi-group data library[9] is used.

The evaluated ^{239}Pu fission cross section set has many energies to represent an excitation function of fission reaction. Though the covariance data might be given for these point-wise cross sections, a group-averaged cross section is sufficient for our uncertainty quantification study for nuclear data applications.

The group-averaged covariance can be obtained by processing the original ENDF

point-wise covariance data with the NJOY code system[10].

It is possible to obtain the group covariance directly from the experimental data by comparing the group-averaged cross sections with the differential measurements. We use a simple Least-Squares fitting procedure[11] with the SOK code[12]. The group-averaged cross sections are compared with experimental differential cross sections in Fig. 1. The experimental data shown here are from many authors but shown by the same symbol, for sake of clarity.

The group-averaged cross section is denoted by a parameter vector $\boldsymbol{x} = (\sigma_1, \sigma_2, \ldots, \sigma_m)^t$ where m is the number of groups taken to be 30 in this study. When the experimental data $\boldsymbol{y} = (\sigma(\epsilon_1), \sigma(\epsilon_2), \ldots, \sigma(\epsilon_n))^t$ are provided, the least-squares solution $\boldsymbol{x}_0$ and its covariance matrix $\mathbf{X}$ are given by

$$\boldsymbol{x}_0 = \mathbf{X}\mathbf{D}^t\mathbf{V}^{-1}\boldsymbol{y}, \tag{1}$$

and

$$\mathbf{X} = \left(\mathbf{D}^t\mathbf{V}^{-1}\mathbf{D}\right)^{-1}, \tag{2}$$

where $\mathbf{V}$ is the covariance of the experimental data taken from the IAEA evaluation, and $\mathbf{D}$ is the design matrix which gives an appropriate interpolation. The covariance $\mathbf{X}$ must be scaled by the ratio χ^2 per degree-of-freedom.

The evaluated uncertainties for the 30-group structure cross sections are shown in Fig. 2 by the solid line. The uncertainties obtained are 1.4% – 2.4% above the unresolved resonance region (the boundary energy is 30 keV), and are reasonable because each data point has typically a 2–6% uncertainty (not shown in Fig. 1), and this uncertainty is reduced by the group-averaging procedure.

The correlation matrix, as shown in Fig. 3, reveals positive correlation coefficients among the group cross sections. In general, the measurements have systematic errors owing to data normalization uncertainty that come from uncertainties in the sample thickness, detector efficiency, etc. In other words, the experimental data may have an unknown normalization arising from those systematic errors. This systematic component in the overall uncertainty leads to a positive correlation among the evaluated cross sections.

Alternatively, the group-averaged covariance can be obtained by processing the original ENDF point-wise covariance data with the NJOY code system[10], if the evaluated covariance data are given[13]. The covariance data in the file are processed with NJOY together with the ERRORJ code[14, 15], which processes resonance parameter covariances, to obtain the covariance matrix for the group cross sections[1]. Although this sequence has an advantage because any group structure can be used, we used the least-squares fitting to generate the group-averaged covariance data as mentioned above, because the evaluated file of ^{239}Pu fission cross section does not contain the covariance.

III INCLUSION OF INTEGRAL DATA

It is known that the ^{239}Pu fission cross section and average number of prompt neutrons ν_p in the LANL nuclear data library predict the $k_{\rm eff}$ value from Jezebel very well (C/E =0.99933). A sensitivity study was carried out for Jezebel. If we increase the ^{239}Pu fission cross section by 1% in the entire energy range, the calculated $k_{\rm eff}$ also increases by about 1%. Recalling the fact that the uncertainties in the ^{239}Pu fission cross section are about 1.5% in the fast region, as shown in Fig. 2, a very simple error estimate for the calculated $k_{\rm eff}$ value might also be 1.5%. This uncertainty is much larger than the experimental uncertainty of Jezebel[2, 3], which is only 0.2%.

To reduce the calculated $k_{\rm eff}$ uncertainty for Jezebel, we adopt a Bayesian update technique, which combines information from differential fission data and the integral data.

In Eqs. (1) and (2), we denoted the 30-group cross sections by the vector $\boldsymbol{x}_0$ and its estimated covariance by $\mathbf{X}$. Providing new information, Jezebel $k_{\rm eff}$ with 0.2% uncertainty, the posterior parameter $\boldsymbol{x}_1$ and its covariance $\mathbf{P}$ are given by[16, 17]

$$\begin{aligned} \boldsymbol{x}_1 &= \boldsymbol{x}_0 + \mathbf{P}\mathbf{C}^t\mathbf{V}^{-1}\left(\boldsymbol{y} - \boldsymbol{f}(\boldsymbol{x}_0)\right), \\ &= \boldsymbol{x}_0 + \mathbf{X}\mathbf{C}^t\left(\mathbf{C}\mathbf{X}\mathbf{C}^t + \mathbf{V}\right)^{-1}\left(\boldsymbol{y} - \boldsymbol{f}(\boldsymbol{x}_0)\right), \qquad (3) \\ \mathbf{P} &= \left(\mathbf{X}^{-1} + \mathbf{C}^t\mathbf{V}^{-1}\mathbf{C}\right)^{-1}, \\ &= \mathbf{X} - \mathbf{X}\mathbf{C}^t\left(\mathbf{C}\mathbf{X}\mathbf{C}^t + \mathbf{V}\right)^{-1}\mathbf{C}\mathbf{X}, \qquad (4) \end{aligned}$$

where $\mathbf{C}$ is the sensitivity matrix, $\boldsymbol{y}$ is the Jezebel experiment, and $\mathbf{V}$ is the covariance of

Jezebel experiment. In this case, there is only one experiment ($k_{\rm eff}$ =1.000 $\pm$ 0.2%), so the matrix $\mathbf{V}$ and vector $\boldsymbol{y}$ become scalars.

The result of the neutron transport calculation using the parameter $\boldsymbol{x}$ is denoted by $\boldsymbol{f}(\boldsymbol{x})$, which is a non-linear function. It can be linearized by the first-order Taylor-series expansion near $\boldsymbol{x}_0$ as

$$\boldsymbol{y} = \boldsymbol{f}(\boldsymbol{x}) \simeq \boldsymbol{f}(\boldsymbol{x}_0) + \mathbf{C}(\boldsymbol{x} - \boldsymbol{x}_0). \tag{5}$$

We refer to this equation as the linear approximation.

Note that Eq. (3) updates the group cross sections, and $\boldsymbol{x}_0$ and $\boldsymbol{x}_1$ are not exactly the same. However the difference is negligible in our case.

Frankle[18] obtained the sensitivity matrix $\mathbf{C}$ by calculating derivatives numerically. PARTISN calculations for Jezebel $k_{\rm eff}$ were performed with an unperturbed and 1% perturbed group cross sections. The sensitivity calculation was performed only for the product $\sigma_i \times \nu_p$. In this study we assume that ν_p has a negligible uncertainty, so that $\delta(\sigma_i \nu_p)$ is $\nu_p \times \delta\sigma_i$. The sensitivity coefficients obtained are shown in Fig. 2 by the dot-dashed line. Since the neutrons in Jezebel have a very hard fast-spectrum with the peak value near 1 MeV, the $k_{\rm eff}$ value is insensitive to the fission cross sections below 10 keV.

Putting the sensitivity coefficients for the 30-group fission cross sections to the Jezebel $k_{\rm eff}$ value into the matrix $\mathbf{C}$ of Eqs. (3) and (4), the adjusted cross sections $\boldsymbol{x}_1$ and their covariance $\mathbf{P}$ are calculated. Although the cross sections $\boldsymbol{x}_0$ and $\boldsymbol{x}_1$ are very similar, as expected, the covariance matrices $\mathbf{X}$ (prior covariance) and $\mathbf{P}$ (posterior covariance) are significantly different. The posterior uncertainties in the cross sections are shown in Fig. 2 by the dotted line. A relatively large reduction in the uncertainty is seen near 1 MeV. The uncertainty estimated with the differential data was 2.4%, and this was reduced to 1.8% by including the integral data. In the other energy regions, however, the reduction is not so large.

The procedure descrbed above is the same as the cross section adjustment that is a popular technique in the nuclear reactor core calculation and dosimetry. The adjustment of cross section always reduces the uncertainties[19]. The main difference of our procedure is that the adjustment aims at obtaining a reasonable cross section set that consistent

with the integral data. On the contrary our procedure does not change the cross section because we know that $k_{\rm eff}$ calculated with the prior set is 1.0, and the change only appears in the covariance.

While the uncertainties in the cross sections in individual groups are only modestly reduced, the biggest benefit of including the integral constraint will be realized for simulations of similar physical setups involving ^{239}Pu and a hard fast-neutron spectrum. A remarkable change can be seen in the correlation matrix shown in Fig. 4, in which negative correlations appear in the fast energy range. These negative correlations come from the constraint imposed by the integral data. They imply that a positive fluctuation in the cross section in one energy group will tend to be accompanied by a decrease in the cross sections in other groups so as to keep an integral quantity constant.

IV UNCERTAINTY QUANTIFICATION OF A SIMULATION USING MONTE CARLO

The posterior covariance matrix $\mathbf{P}$ discussed in the preceding section provides a description of the uncertainties in the group cross sections. The posterior probability distribution for the cross section vector $\boldsymbol{x}$ is proportional to $\exp\{-(1/2)(\boldsymbol{x}-\boldsymbol{x}_1)^t\mathbf{P}^{-1}(\boldsymbol{x}-\boldsymbol{x}_1)\}$. With this distribution, we can use a Monte-Carlo technique to estimate the uncertainty in simulations of related physical phenomena. The general approach is to draw random samples of $\boldsymbol{x}$ from its probability distribution, and use each sample in the simulation to calculate its associated output. The ensemble of outputs can be used to characterize their uncertainties. We illustrate this technique by estimating the uncertainty in the simulation of the same Jezebel experiment we used above.

The first step in the Monte Carlo technique is to draw random samples from the probability distribution with the specified covariance matrix, either $\mathbf{X}$ or $\mathbf{P}$ given by Eqs. (2) and (4). We first diagonalize the covariance matrix by subjecting it an eigenanalysis. This analysis also provides a good test of the positive-definiteness of covariance matrix. We confirmed that our covariance matrices are both positive-definite. In the eigenvector space, the covariance matrix is diagonal, meaning the eigenvalues are uncorrelated. We

draw 30 independent random samples from a Gaussian distribution with unit variance. After multiplication by the square root of the eigenvalues, this vector is transformed into the cross-section space to obtain the correlated fluctuations in the samples about the mean value $\boldsymbol{x}_1$. The last steps are repeated again and again to obtain more random samples.

The covariance matrix $\mathbf{P}$ (or $\mathbf{X}$) can be diagonalized as:

$$\mathbf{U}^{-1}\mathbf{P}\mathbf{U} = \mathrm{diag}(\lambda_1, \lambda_2, \ldots, \lambda_m), \tag{6}$$

where λ's are the eigenvalues of the covariance matrix $\mathbf{P}$, and the matrix $\mathbf{U}$ contains the eigenvector $(u_{1i}, u_{2i}, \ldots, u_{mi},)^t$ for the i-th eigenvalue λ_i.

In the eigenvector space, there is no off-diagonal element in the covariance matrix, so we sample the eigenvalues ξ_i from the Gaussian distributions with the standard deviation of $\sqrt{\lambda_i}$, and the center value of zero. The distribution of ξ_i is given by

$$p(\xi_i)d\xi_i = \frac{1}{\sqrt{2\pi\lambda_i}} \exp\left(-\frac{\xi_i^2}{2\lambda_i}\right) d\xi_i, \tag{7}$$

with $\langle\xi_i\rangle = 0$ and $\langle\xi_i^2\rangle = \lambda_i$.

When the sampled values ξ_i are provided, an element of $\mathbf{P}$, $p_{ij} = \mathrm{cov}(\sigma_i, \sigma_j)$, can be calculated as

$$\begin{aligned} p_{ij} = \sum_k u_{ik}u_{jk}\lambda_k &= \sum_k u_{ik}u_{jk}\langle\xi_k^2\rangle \\ &= \left\langle \sum_k u_{ik}u_{jk}\xi_k^2 \right\rangle \\ &= \left\langle \sum_k u_{ik}\xi_k \sum_k u_{jk}\xi_k \right\rangle. \end{aligned} \tag{8}$$

Here we used $\langle u_{ik_1}\xi_{k_1}u_{jk_2}\xi_{k_2}\rangle = u_{ik_1}u_{jk_2}\langle\xi_{k_1}\xi_{k_2}\rangle = 0$ for $k_1 \neq k_2$.

From Eq. (8), $\sum_k u_{ik}\xi_k$ is a deviation from an averaged cross-section when the eigenvalue ξ_k is sampled :

$$\sigma_i' = \sigma_i + \delta\sigma_i = \sigma_i + \sum_k u_{ik}\xi_k, \tag{9}$$

where σ_i' can be used as the sampled set. In fact,

$$\mathrm{cov}(\sigma_i', \sigma_j') = \langle\delta\sigma_i\delta\sigma_j\rangle = \left\langle \sum_k u_{ik}\xi_k \sum_k u_{jk}\xi_k \right\rangle = p_{ij}. \tag{10}$$

Therefore the covariance of sampled cross-section set $\{\sigma_i'\}$ is equal to $\mathbf{P}$.

Figure 5 shows an example of the Monte Carlo realization based on the matrix $\mathbf{X}$ in Eq. (2). Two random samples (dot-dashed, and dashed lines) are shown here together with the unperturbed cross section by the solid line. Because the matrix $\mathbf{X}$ has positive correlations, the randomly-sampled cross sections tend to move in the same direction. Such a tendency can be seen in the cross section set shown by dashed line, which is systematically lower than the unperturbed cross section.

The Monte Carlo realization based on the matrix $\mathbf{P}$ in Eq. (4) is shown in Fig. 6. The sampled cross sections look less correlated than those in Fig. 5, as we expect from the negative correlations in the matrix $\mathbf{P}$.

Before we perform a real neutron transport calculation with our ensemble, we have simulated the $k_{\rm eff}$ prediction for Jezebel by using the linear approximation to PARTISN calculations, which is expressed by Eq. (5), or more specifically given by

$$k_{\rm eff}^{(n)} \simeq k_{\rm eff}^{(0)} + \mathbf{C}(\boldsymbol{x}_n - \boldsymbol{x}_0), \tag{11}$$

where $\boldsymbol{x}_0$ and $\boldsymbol{x}_n$ are the unperturbed and n-th sampled cross sections, respectively, and $k_{\rm eff}^{(0)}$ is the calculated $k_{\rm eff}$ value with $\boldsymbol{x}_0$ cross section.

We have generated 1000 samples to reproduce the uncertainty distribution of $k_{\rm eff}$, which is shown in Fig. 7. The solid histogram shows the distribution of $k_{\rm eff}$ when the covariance matrix $\mathbf{X}$ is used. The dotted histogram is for the case of matrix $\mathbf{P}$. Both distributions are approximated well by a Gaussian of σ =0.8% and 0.2%, respectively. We also calculated the uncertainties in k_{eff} using the standard error propagation technique, and obtained exactly the same answers. The uncertainty in the Jezebel experiment, 0.2%, is well reproduced by this simulation. It is clearly seen that the integral data reduce the uncertainty in the $k_{\rm eff}$ prediction. From the uncertainty in the fission cross section for ^{239}Pu, we reiterate that the uncertainty from the transport method used for the calculation is not considered here.

As a full neutron transport calculation, we have performed the PARTISN calculation for Jezebel with 30 samples. The result is shown in Fig. 8. Note that the width of each histogram is different from that in Fig. 7.

We have compared the simulated k_{eff} obtained with the linear approximation and the real PARTISN calculation, and found that they agree up to 5 digits (the difference is less than 0.01%). That means that if we perform the PARTISN calculations for 1000 samples, we may obtain the same distributions in Fig. 7. The Monte Carlo method also includes a higher-order effect, but the agreement with the linear (first order) approximation shows that the higher-order effect is neglegible in our case.

As seen in Fig. 8, the most probable value is distributed around 1.0, but 30 samples are insufficient to adequately represent the Gaussian distribution, although the uncertainty reduction can be clearly seen in this figure too. It is probably possible to carry out the PARTISN calculation for more samples within a realistic computational time, but other neutron transport calculations, such as a Monte Carlo simulation, are very difficult to perform so many times. This issue could become critical for many applications for which the uncertainty quantification study is needed. Advanced techniques[20] for sampling may reproduce the Gaussian distribution with fewer samples. These techniques employ rather more uniformly distributed random numbers than the standard random Monte Carlo method to reduce the number of samples required to achieve a given accuracy. To apply our Monte Carlo uncertainty quantification method to time-consuming computer codes, advanced sampling techniques, such as quasi-Monte Carlo, need to be incorporated.

V CONCLUSION

We presented a Monte Carlo technique to perform uncertainty quantification for nuclear applications, combining the covariance evaluation of differential cross-sections data and the error propagation from matching the Jezebel experiment using the PARTISN neutron-transport calculation. This technique does not address the uncertainty for a calculated value based on the transport method used in a given calculation.

The covariance of ^{239}Pu fission cross section was estimated from the experimental differential data. The evaluation of ^{239}Pu differential cross-section data was then combined with the integral data of the Jezebel critical assembly using the Bayesian method, hence reducing the uncertainties in the fission cross sections.

Random samples of the fission cross sections were generated based on the covariance matrices obtained, and distributions of the neutron multiplicity, k_{eff}, were estimated. It was shown that the experimental uncertainty of Jezebel, which is 0.2%, was well reproduced by including the integral data into the covariance of ^{239}Pu fission cross section.

ACKNOWLEDGMENT

We are grateful to Dr. V. Pronyaev of IAEA Nuclear Data Section and Dr. A.D. Carlson of NIST for providing the experimental database used for the standard evaluations at IAEA.

REFERENCES

1. M. ISHIKAWA, "Development of a Unified Cross-Section Set ADJ2000 Based on Adjustment Technique for Fast Reactor Analysis," *J. Nucl. Sci. Technol.,* **Suppl.2**, 1073 (2002).

2. S.D. CLEMENT, *Nucl. Sci. Eng.,* **145**, 72 (2003).

3. "International Handbook of Evaluated Criticality Safety Benchmark Experiment," NEA/NSC/DOC(95)03, Organisation for Economic Co-operation and Development / Nuclear Energy Agency (2002).

4. Bayesian technique, need ref.

5. "PARTISN," Transport Methods Group, CCS-4, Los Alamos National Laboratory, Los Alamos National Laboratory, LA-UR-02-5633 (2002).

6. P. TALOU, M.B. CHADWICK, D. MADLAND, P.G. YOUNG, "Modification of ENDF/B-VI Release 5 (MOD 5) (pu239la7d)," Los Alamos National Laboratory (2003) [private communication].

7. A.D. CARLSON, G.M. HALE, V.G. PRONYAEV, "Summary Report of the 3rd IAEA Research Co-ordination Meeting on Improvement of the Standard Cross Sections," Vienna, 18–22 October 2004, INDC(NDS)-463 (2004).

8. A.D. CARLSON, G.M. HALE, V.G. PRONYAEV, "Summary Report of the Second Research Co-ordination Meetings on Improvement of the Standard Cross Sections for Light Elements," Gaithersburg, MD, USA, 13–17 October 2003, INDC(NDS)-453 (2004).

9. R.C. LITTLE, "MENDF6: A 30-Group Neutron Cross-Section Library Based on ENDF/B-VI," Los Alamos National Laboratory, LA-UR-98-545 (1998).

10. R.E. MACFARLANE, D.W. MUIR, "The NJOY Nuclear Data Processing System Version 91," Los Alamos National Laboratory, LA-12740-M (1994).

11. Least-squares technique, need ref.

12. T. KAWANO, H. MATSUNOBU, T. MURATA, A. ZUKERAN, Y. NAKAJIMA, M. KAWAI, O. IWAMOTO, K. SHIBATA, T. NAKAGAWA, T. OHSAWA, M. BABA, T. YOSHIDA, *J. Nucl. Sci. Technol.,* **37**, 327 (2000).

13. K. SHIBATA, A. HASEGAWA, O. IWAMOTO, S. CHIBA, M. SUGIMOTO, N. ODANO, T. KAWANO, Y. NAKAJIMA, T. MURATA, H. MATSUNOBU, S.Y OH, K. YOKOYAMA, K. SUGINO, M. ISHIKAWA, K. KOSAKO, N. YAMANO, Y. KANDA, "JENDL-3.2 Covariance File," *J. Nucl. Sci. Technol.,* **Suppl.2**, 40 (2002).

14. K. KOSAKO, N. YAMANO, "Preparation of a Covariance Processing System for the Evaluated Nuclear Data File, JENDL, (III)," JNC TJ 9440 99-003 (1999) [in Japanese]; K. KOSAKO, "Covariance Data Processing code: ERRORJ," *Proc. of the Specialists' Meeting on Reactor Group Constants,* Feb. 22–23, 2001, JAERI, Tokai, Japan, edited by J. Katakura, JEARI-Conf 2001-009 (2001) pp.30–34.

15. G. CHIBA, M. ISHIKAWA, "Revision and Application of the Covariance Data Processing Code, ERRORJ," *Proc. Int. Conf. Nuclear Data for Science and Technology,* Sep.26–Oct.1, 2004, Santa Fe, New Mexico, USA, [in press (2005)].

16. T. KAWANO, K. SHIBATA, "Covariance Evaluation System," JAERI-Data/Code 97-037, (1997) [in Japanese].

17. T. KAWANO, *Nucl. Sci. Eng.,* **131**, 107 (1999).

18. S.C. FRANKLE, "Results of Initial Jezebel Calculations for Testing the Sensitivity of $k$eff Calculations to Changes in $\overline{\nu}\sigma_f$," Los Alamos National Laboratory, LA-UR-05-1457 (2005).

19. R.L. PEREL, J.J. WAGSCHAL, Y. YEIVIN, "pV-Surveillance Dosimetry and Adjustment: Review of Several Significant Oral Laws," Reactor Dosimetry: Radiation Metrology and Assessment, ASTM STP 1398, Ed. J.G. Williams, D.W. Vchar, F.H.

Ruddy, and D.M. Gilliam, American Society for Testing and Materials, West Conshohocken, 486 (2001).

20. T.J. SANTNER, B.J. WILLIAMS, N.I. NOTZ, "Design and Analysis of Computer Experiments," Springer, New York (2003).

Fig. 1: Comparison of the ^{239}Pu fission cross sections in the 30-group structure with differential experimental data. All group averages include numerous measurements but shown by the same symbol.

Fig. 2: RMS uncertainties in the ^{239}Pu fission cross sections. The solid line is the result that includes differential measurements only, the dotted line is the case in which Jezebel integral data are added, and the dot-dashed line shows a relative sensitivity of group-cross sections to k_{eff} value (right axis).

Fig. 3: Correlation matrix for the ^{239}Pu fission cross sections, evaluated based on the differential measurements only.

Fig. 4: Correlation matrix for the ^{239}Pu fission cross sections, evaluated based on both differential and integral data. The area surrounded by the solid rectangle has a negative correlation.

Fig. 5: An example of Monte Carlo realization for the ^{239}Pu fission cross sections. The sold line indicates the unperturbed fission cross sections; the dotted and dot-dashed lines show two random samples from the covariance matrix based on the differential data.

Fig. 6: Same as Fig. 5, but for the case in which the Jezebel integral data are included.

Fig. 7: Distributions of simulated k_{eff} prediction for Jezebel. The linear approximation was used. The solid histogram shows the distribution of k_{eff} when the prior covariance matrix $\mathbf{X}$ is used. The dotted histogram is for the posterior covariance matrix $\mathbf{P}$.

Fig. 8: Distributions of calculated k_{eff} values for Jezebel with the PARTISN code. The solid histogram shows the distribution of k_{eff} when the prior covariance matrix $\mathbf{X}$ is used. The dotted histogram is for the posterior matrix $\mathbf{P}$.

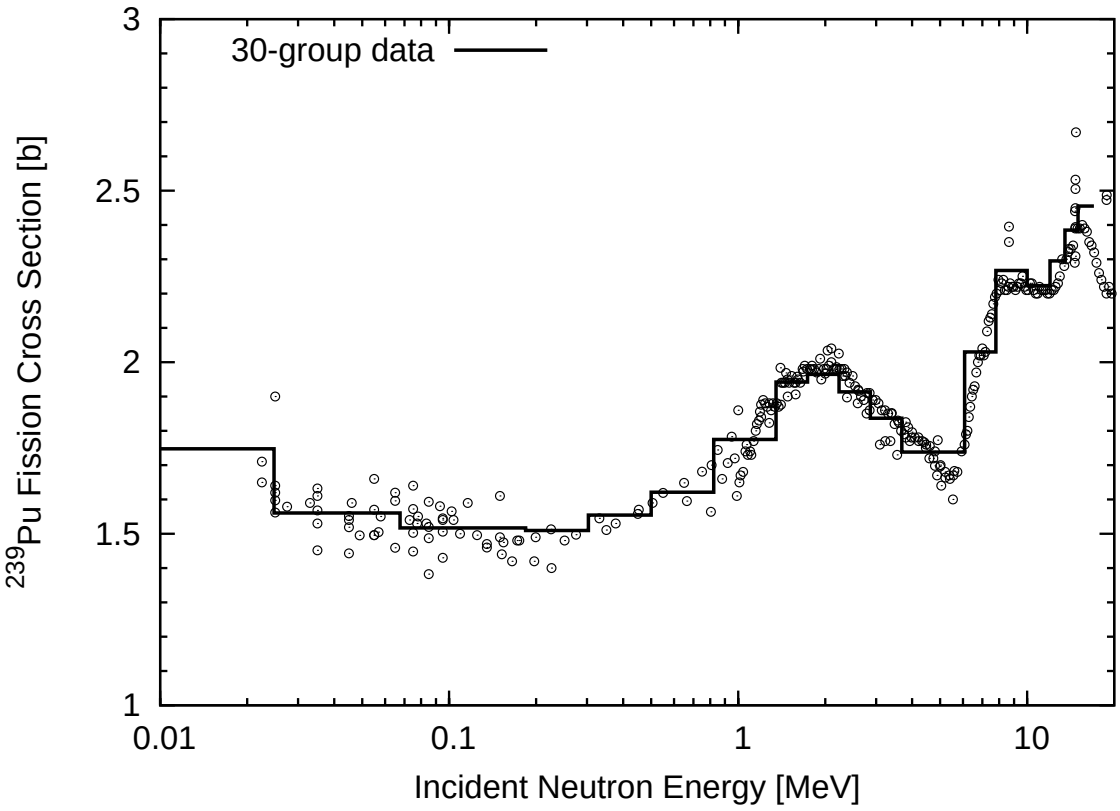

Fig. 1, Combination of differential and integral . . .T. Kawano

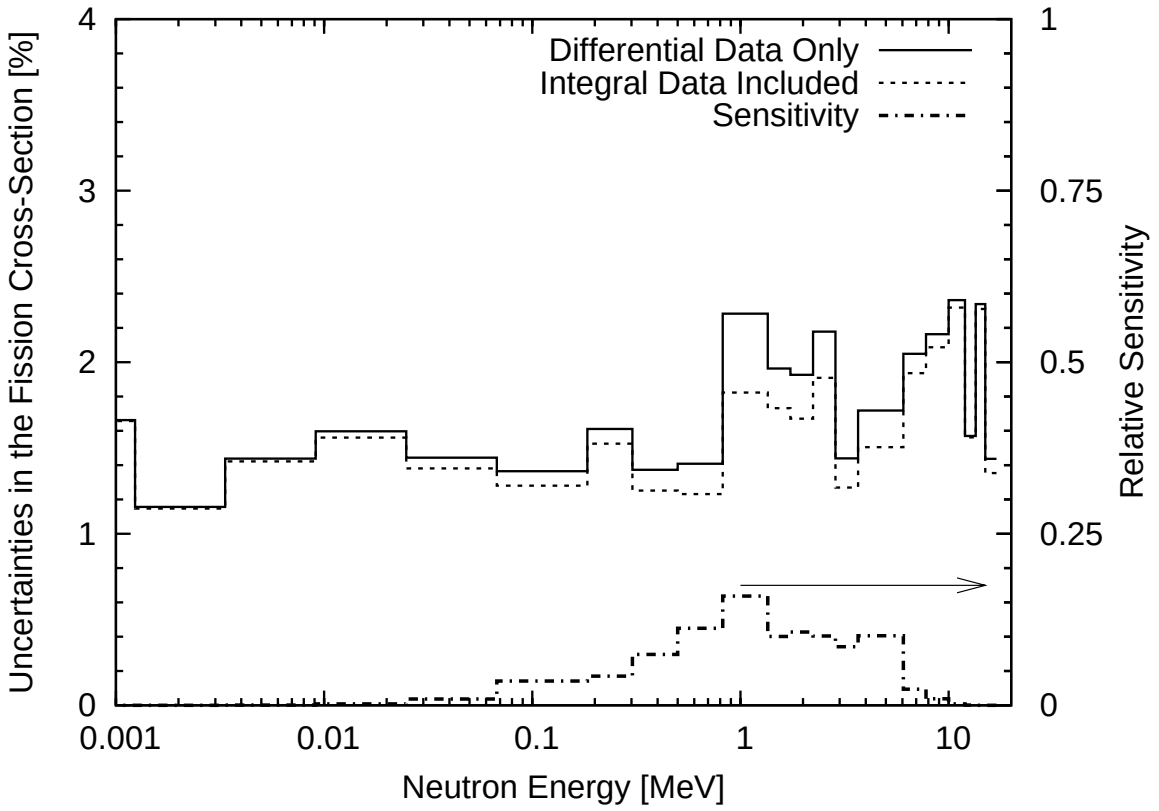

Fig. 2, Combination of differential and integral . . .T. Kawano

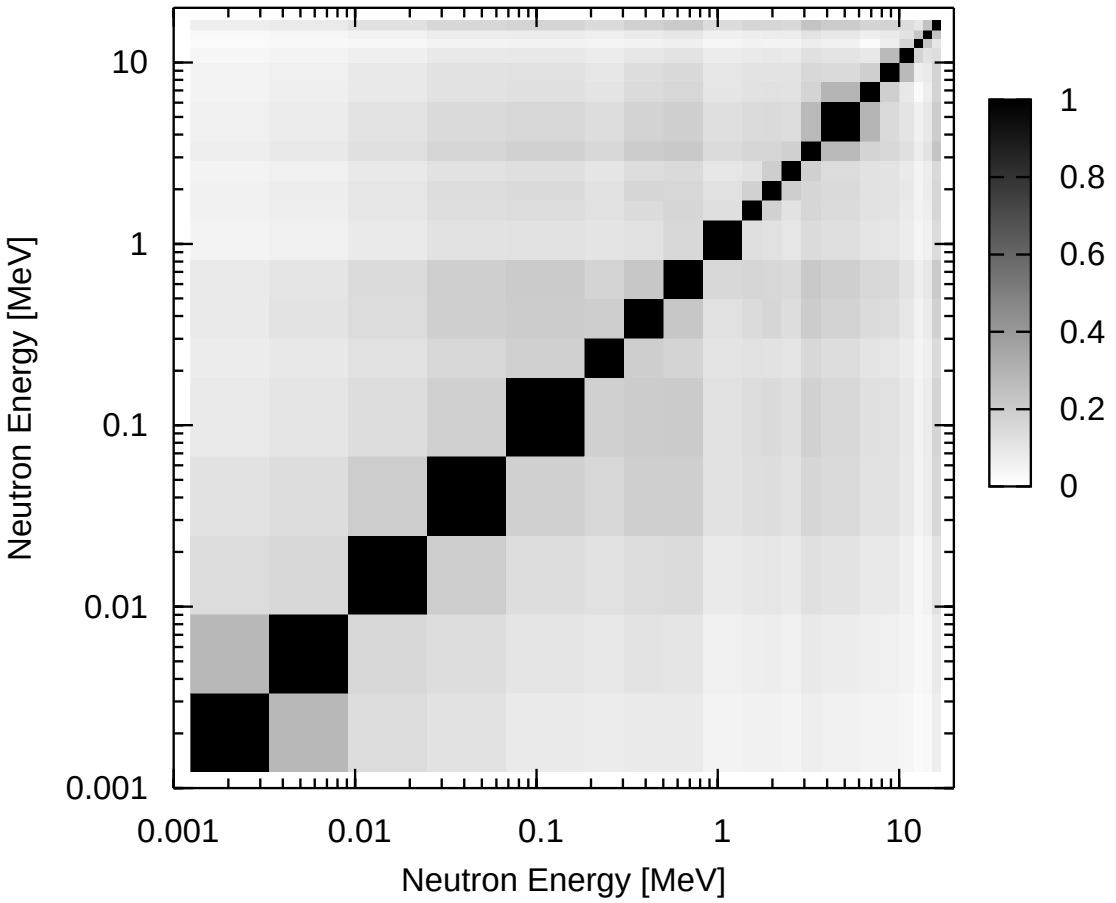

Fig. 3, Combination of differential and integral ...T. Kawano

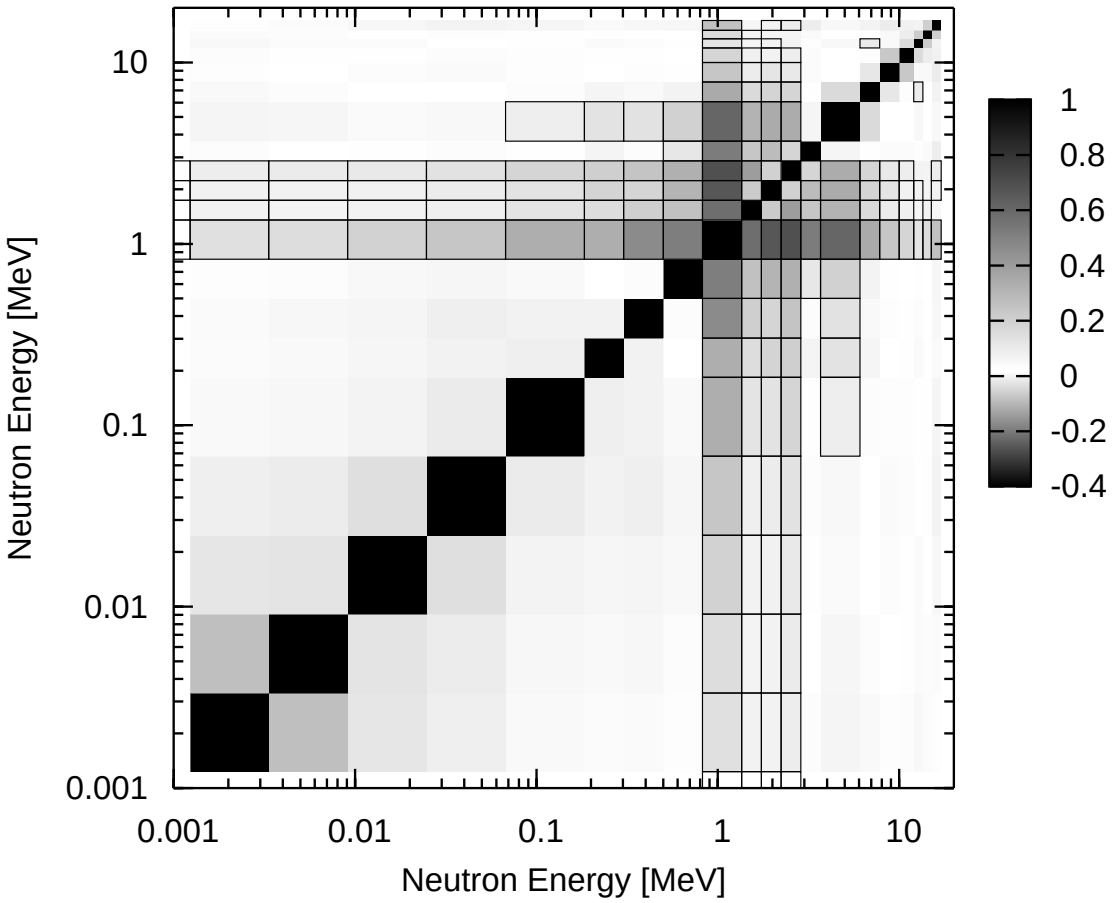

Fig. 4, Combination of differential and integral ...T. Kawano

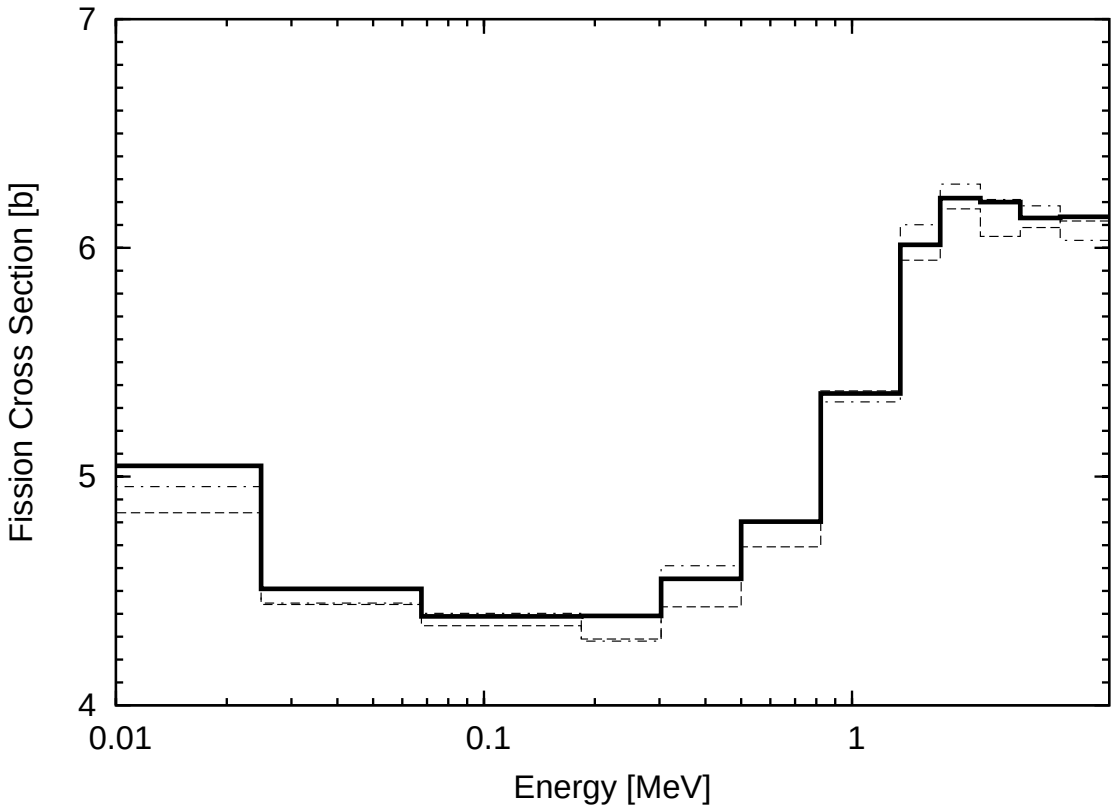

Fig. 5, Combination of differential and integral . . .T. Kawano

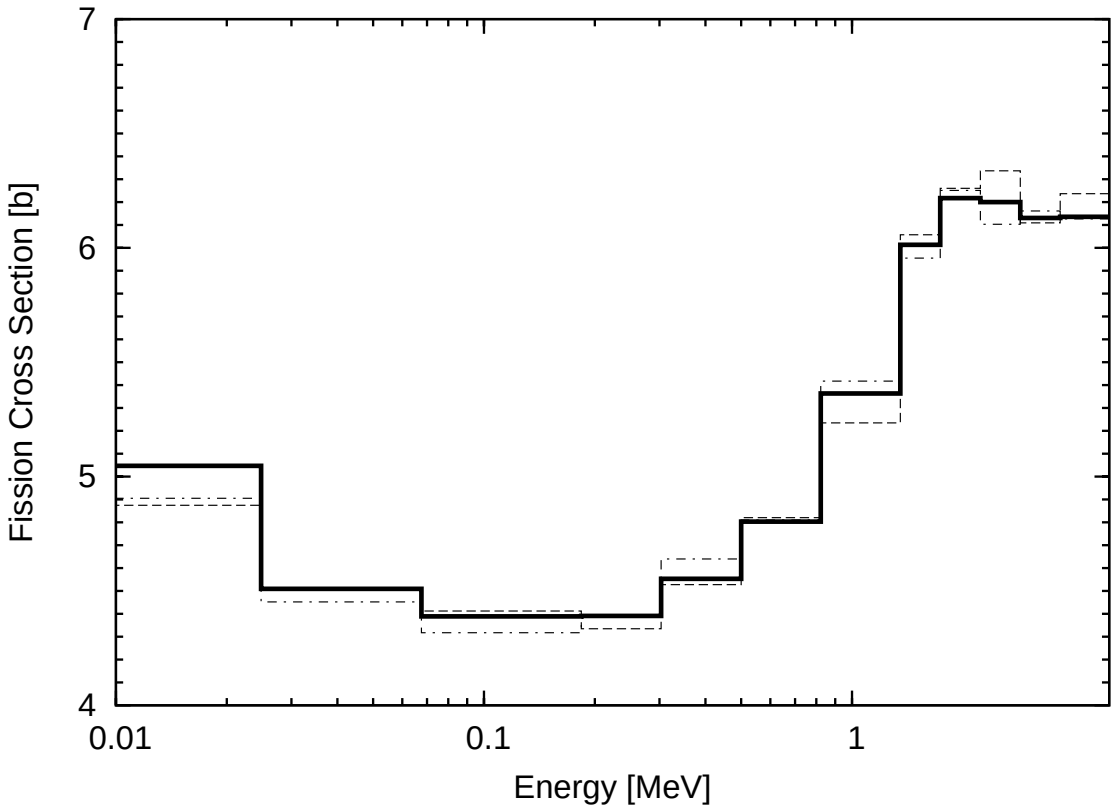

Fig. 6, Combination of differential and integral . . .T. Kawano

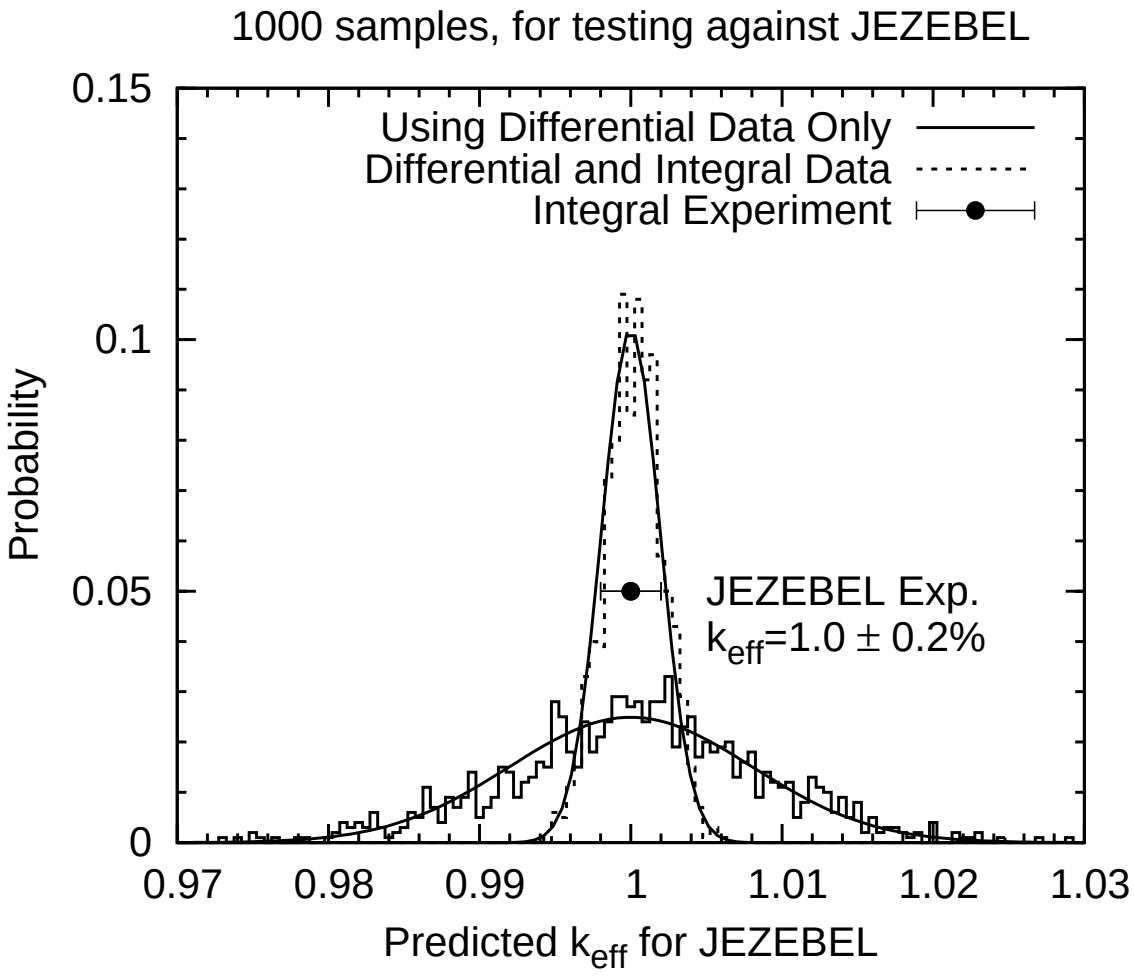

Fig. 7, Combination of differential and integral . . .T. Kawano

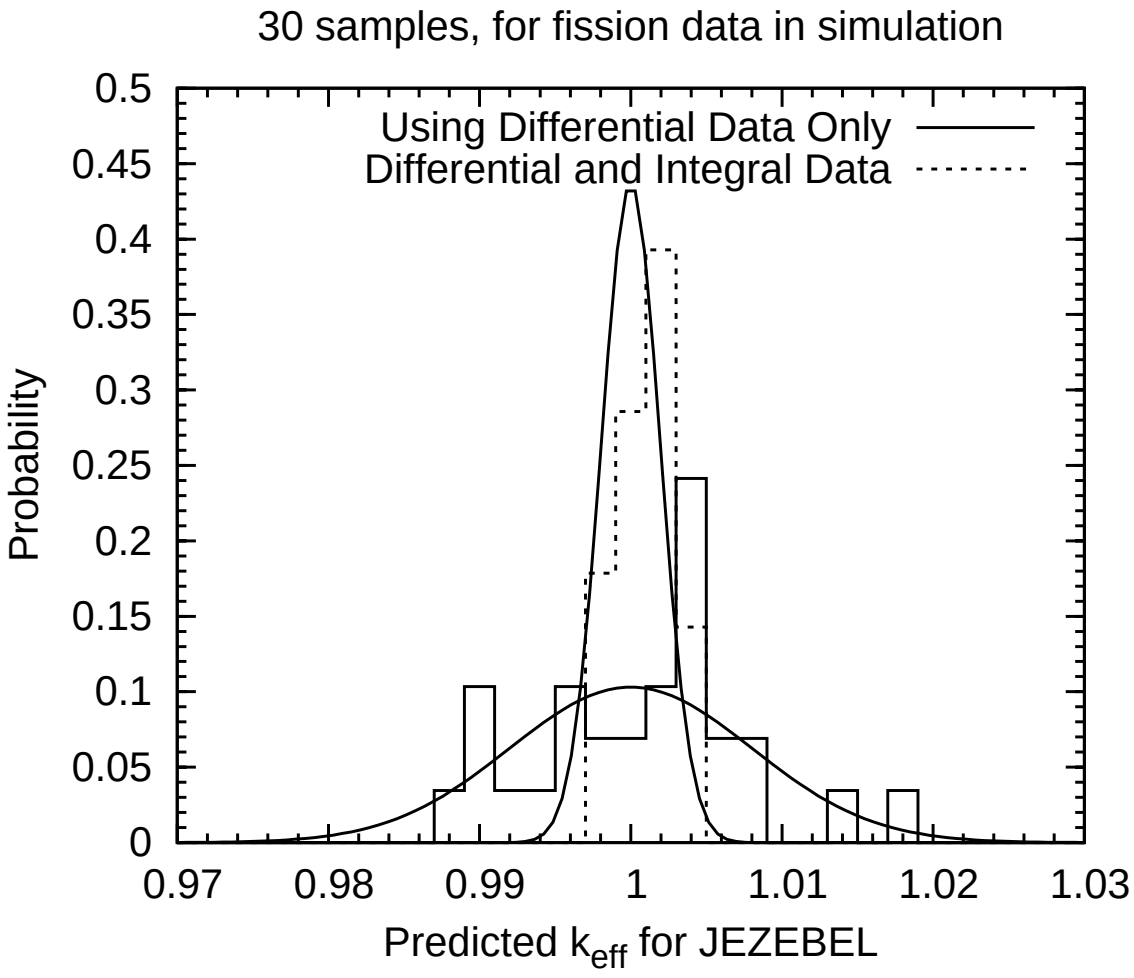

Fig. 8, Combination of differential and integral . . .T. Kawano